Monthly Notices
of the
ROYAL ASTRONOMICAL SOCIETY

MNRAS **495,** 1566–1576 (2020) doi:10.1093/mnras/staa1189

Study of flux-rope characteristics at sub-astronomical-unit distances using the *Helios* 1 and 2 spacecraft

Anil Raghav [1]★ Sandesh Gaikwad,[1] Yuming Wang,[2]★ Zubair I. Shaikh [3] Wageesh Mishra[2,4] and Ake Zao[5]

[1] *University Department of Physics, University of Mumbai, Vidyanagari, Santacruz (E), Mumbai-400098, India*
[2] *CAS Key Laboratory of Geospace Environment, Department of Geophysics and Planetary Sciences, University of Science and Technology of China, Hefei, China*
[3] *Indian Institute of Geomagnetism (IIG), New Panvel, Navi Mumbai-410218, India*
[4] *Max Planck Institute for Solar System Research, Justus-von-Liebig-Weg 3, 37077, Göttingen, Germany*
[5] *College of Physics and Electric Information, Luoyang Normal University, Luoyang, Henan 471934, China*

Accepted 2020 April 23. Received 2020 April 23; in original form 2019 December 23

ABSTRACT

Magnetic flux ropes observed as magnetic clouds near 1 au have been extensively studied in the literature and their distinct features are derived using numerous models. These studies summarize the general characteristics of flux ropes at 1 au without providing an understanding of the continuous evolution of the flux ropes from near the Sun to 1 au. In the present study, we investigate 26 flux ropes observed by the *Helios* 1 and 2 spacecraft (from 0.3 to 1 au) using the velocity-modified Gold–Hoyle model. The correlation and regression analyses suggest that the expansion speed, poloidal speed, total magnetic helicity and twist per au of the flux rope are independent of heliospheric distance. The study implies that the aforementioned features are more strongly influenced by their internal properties compared with external conditions in the ambient medium. Moreover, the poloidal magnetic flux and magnetic energy of the studied flux ropes exhibit power-law dependence on heliospheric distance. A better understanding of the underlying physics and corroboration of these results is expected from the *Parker Solar Probe* measurements in the near future.

Key words: Sun: coronal mass ejections – solar–terrestrial relations – solar wind.

1 INTRODUCTION

Magnetic flux ropes are universal structures in the space plasma consisting of twisted magnetic field lines winding around a common axis. They are core structures of coronal mass ejections (CMEs), which play a crucial role in heliospheric dynamics and various solar–terrestrial effects including extreme space weather conditions near the Earth (Burlaga 1988; Priest 1990; Schwenn 2006; Moldwin 2008; Raghav et al. 2017, 2018; Shaikh, Raghav & Bhaskar 2017). The most commonly observed flux rope structure at 1 au is the magnetic cloud, which is a subset of interplanetary counterparts of coronal mass ejections (ICMEs; Burlaga et al. 1981; Goldstein 1983; Marubashi 1986; Gosling 1990; Burlaga 1991; Farrugia et al. 1993; Bothmer & Schwenn 1994; Farrugia et al. 2005; Leitner et al. 2007; Kilpua, Koskinen & Pulkkinen 2017).

Various studies in the past have established that magnetic clouds are loop-like coherent magnetic flux ropes whose two ends are rooted in the Sun (Zhang & Burlaga 1988; Larson et al. 1997). The magnetic clouds are known to show a large and smooth rotation of the magnetic field vectors as seen in *in situ* observations near Earth (Burlaga et al. 1981). In addition to flux rope observations at 1 au, some efforts have also been made to study them at different locations in interplanetary space (Moldwin et al. 1995; Gulisano et al. 2012). Recently Owens, Lockwood & Barnard (2017) proposed that flux ropes can be non-coherent in nature beyond approximately 0.3 au from the Sun. In fact, various *in situ* and coronagraphic observations as well as different models have been utilized to visualize their topographic evolution in interplanetary space. Basically, a study of the evolution of magnetic flux ropes serves two main purposes: (i) to reconstruct a realistic geometry and magnetic field configuration (Goldstein 1983; Marubashi 1986; Burlaga 1988; Lepping, Jones & Burlaga 1990; Mulligan & Russell 2001; Hu & Sonnerup 2002; Vandas & Romashets 2003; Romashets & Vandas 2003; Hidalgo & Nieves-Chinchilla 2012; Al-Haddad et al. 2011, 2013); (ii) to understand the expansion and distortion of the cross-section of a magnetic cloud (e.g. Farrugia et al. 1993; Farrugia, Osherovich & Burlaga 1995; Marubashi 1997; Shimazu & Vandas 2002; Berdichevsky,

★ E-mail: raghavanil1984@gmail.com (AR); ymwang@ustc.edu.cn (YW)

Lepping & Farrugia 2003; Hidalgo 2003; Owens, Merkin & Riley 2006; Dasso et al. 2007; Démoulin & Dasso 2009a, b; Démoulin, Dasso & Janvier 2013; Raghav & Shaikh 2020).

The simplest and most widely used model to understand the flux rope is a cylindrical linear force-free field model also referred to as the Lundquist model (Goldstein 1983; Burlaga 1988; Lepping et al. 1990). Moreover, non-circular cross-section models (Vandas & Romashets 2003; Démoulin & Dasso 2009a) or non-linear force-free models (Mulligan & Russell 2001; Hidalgo & Nieves-Chinchilla 2012; Wang et al. 2015, 2016) have been developed to understand the more precise geometric information of the flux rope. In all these models, curvature information about the flux rope was missing. This has led to the development of the toroidal geometry model that keeps an invariance along the axis, which causes a large number of free parameters in the model. However, it has not yet been demonstrated how well the data from a single spacecraft can constrain the free parameters, especially the local curvature of the axis, which is important for obtaining the global shape of the flux-rope axis (e.g. Marubashi 1997; Romashets & Vandas 2003; Marubashi & Lepping 2007; Romashets & Vandas 2009; Owens et al. 2012; Marubashi et al. 2012). Nakagawa & Matsuoka (2010) suggested that the toroidal model can be applied to observations of a flux rope from well-separated spacecraft, as the observations from multiple viewpoints provide more constraints on this model. Furthermore, Hu & Sonnerup (2002) have used the Grad–Shafranov (GS) technique to study two-dimensional flux-rope geometry and have found that a flux rope has a nearly circular cross-section at 1 au.

The expansion of a flux rope during its propagation away from the Sun has been reported in earlier studies (Berdichevsky et al. 2003; Wang, Du & Richardson 2005; Jian et al. 2006; Gulisano et al. 2010). The anisotropic expansion of the flux rope may lead to the distortion of the initially circular cross-section geometry into a non-circular shape. However, various models suggest that the flux-rope cross-section is not far from a circular shape (Hidalgo 2003). Further, the statistical studies by Wang et al. (2002, 2004, 2006, 2014), Kilpua et al. (2009), Lugaz (2010), Isavnin, Vourlidas & Kilpua (2013) and Isavnin, Vourlidas & Kilpua (2014) suggest a deflection of the ICME in interplanetary space. In addition to the propagation and expansion speed of the flux ropes, Wang et al. (2015) have suggested the existence of poloidal speed of the plasma within the flux rope. Besides the dynamic evolution of the flux rope, the build-up and distribution of twist within the flux rope is also of interest. The twists of magnetic field lines inside a large-scale flux-rope structure can be determined using energetic particles (Larson et al. 1997; Kahler, Krucker & Szabo 2011), multiwavelength observations of the flux rope during its formation (Wang et al. 2017), and modelling studies using the *in situ* observations of the flux rope, such as a GS reconstruction technique and/or a uniform-twist flux rope with a Gold–Hoyle (GH) solution (e.g. Farrugia et al. 1999; Hu & Sonnerup 2002; Dasso et al. 2006; Hu et al. 2014; Hu, Qiu & Krucker 2015; Wang et al. 2016, 2018; Zhao et al. 2018). The average twist may be changed by the erosion of the flux rope during its evolution in interplanetary space (Wang et al. 2018). Hood & Priest (1981) proposed that when the total twist angle exceeds 2.5π radians (i.e. the total number of turns exceeds the critical twist limit of 1.25), the flux rope becomes kink-unstable. However, Wang et al. (2016) suggested that most of the flux ropes observed near Earth as magnetic clouds have a total twist larger than 10π radians (i.e. total turns more than 5), which is much higher than the theoretically suggested value of critical twist. They suggested that the critical twist of a flux rope is proportional to the aspect ratio of the flux rope (i.e. the ratio of the length of the flux-rope axis to the radius of the cross-section of the flux rope). It is very exciting to study the properties of flux ropes in sub-astronomical-unit (sub-au) and super-au regions of interplanetary space and further to compare them with the well-studied properties of the flux ropes observed at 1 au. In the present study, we study the properties of flux ropes observed as magnetic clouds by the *Helios* 1 and 2 spacecraft at different locations ranging between 0.38 and 0.96 au in the inner heliosphere. For this purpose, we apply the velocity-modified Gold–Hoyle (VMGH) model, as discussed by Wang et al. (2016), to the *in situ* observations of the *Helios* 1 and *Helios* 2 spacecraft. Our study demonstrates the heliospheric evolution of the flux-rope properties and provides a global picture of a flux rope associated with an erupting CME from the Sun.

2 VELOCITY-MODIFIED GOLD–HOYLE MODEL

This model considers a magnetic flux rope as a loop-like structure and uses a cylindrical coordinate (r, φ, z) system to investigate the properties of the flux-rope segment. A detailed description of the model is given in Wang et al. (2016). The fitting optimization procedure of the VMGH model is discussed in detail by Wang et al. (2015). We have utilized exactly the same free parameters as used by Wang et al. (2016). The model estimates various physical properties of the flux rope, such as expansion speed, poloidal speed, twist, helicity, magnetic flux energy, orientation of the flux-rope axis and dimensions of the flux rope, etc. These are very important to understand the dynamic and structural evolution of the flux rope from the solar corona into the heliosphere. We have identified 26 cases of flux ropes observed by *Helios*, and the detailed procedure of our analysis is explained for a typical case, as described in Section 2.1. In our study, we also apply the model to other cases to make the same analysis.

2.1 Model application to a typical event

We have utilized the following criteria, as discussed by Bothmer & Schwenn (1998) and Burlaga (1991), to identify magnetic clouds in *Helios* 1 and 2 data at distances from 0.3 to 1 au: (i) rotation of the interplanetary magnetic field in any direction relative to the ecliptic plane for large time intervals; (ii) high magnetic field strength compared with the ambient field; (iii) low temperature inside the magnetic cloud with respect to ambient temperature. The criteria (ii) and (iii) automatically fulfil a low plasma beta value inside the magnetic cloud (Klein & Burlaga 1982). Note that, for an individual magnetic cloud, all three criteria must be satisfied simultaneously.

Fig. 1 demonstrates a typical flux-rope event observed by the *Helios* 1 spacecraft on 1975 January 7, which is fitted with the VMGH model. The superimposed black solid lines on *in situ* plasma parameters are the best-fitting curves derived from the VMGH model (Wang et al. 2016). Note that all the free parameters of the model (except for ω) were calculated and optimized using a least-squares fitting procedure by taking series of initial values. A detailed description of the procedure is given in section 2.1.3 of Wang et al. (2015). Further, the value of ω is calculated using $\omega_i = B_{i\phi}/x_i B_{iz}$, where B_ϕ and B_z are measured magnetic field vectors and x is the normalized distance from the axis of the magnetic flux rope. The ω_i equation depends on the elevation (θ) and azimuth (ϕ) angle of the axis of the flux rope at the closest approach, d (Wang et al. 2016). We calculated ω_i for all data points associated with the magnetic

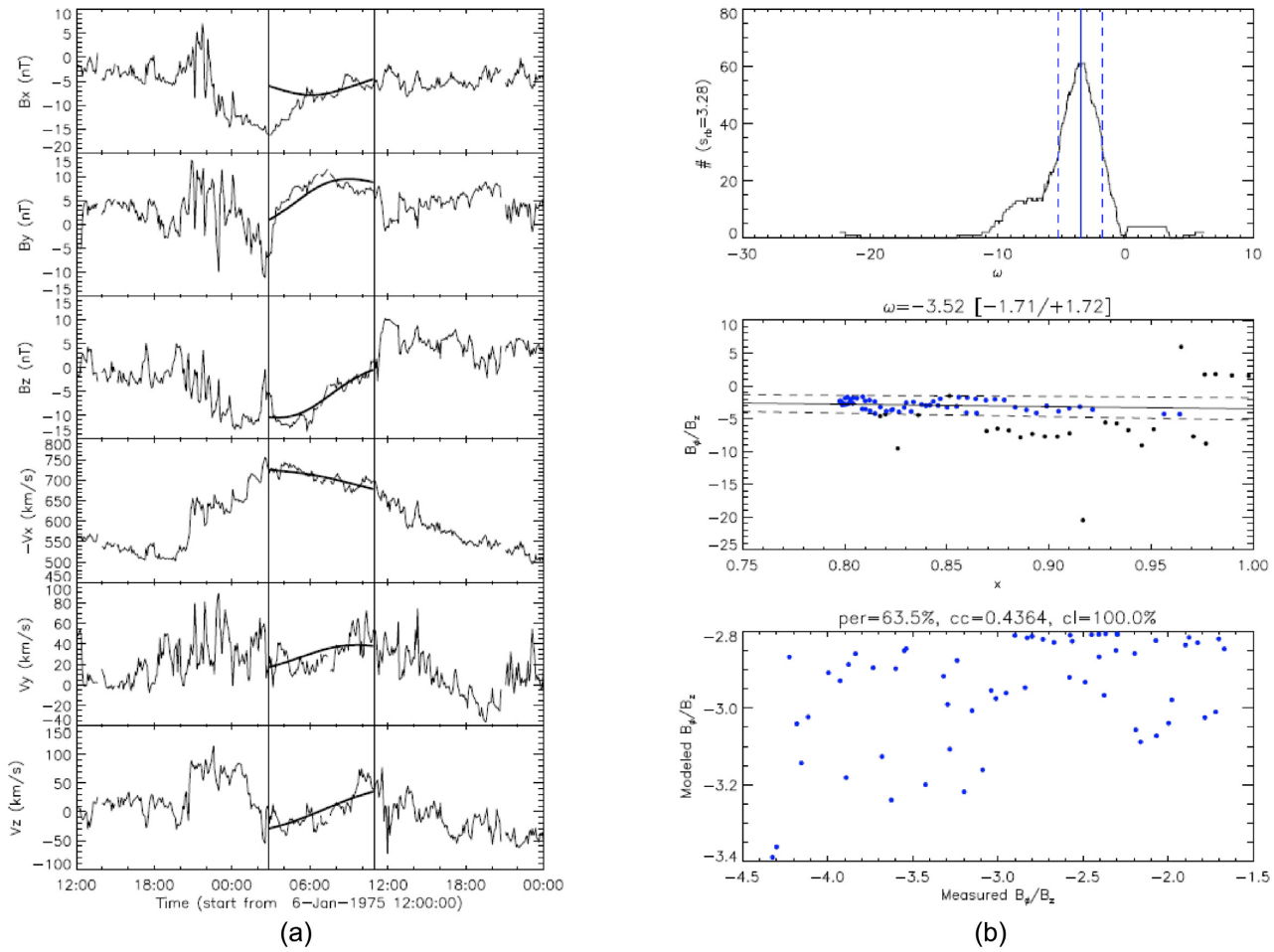

Figure 1. Left: the temporal variation of the interplanetary magnetic field and solar wind velocity observed by the *Helios* spacecraft for the selected flux rope (in GSE coordinates). The vertical black solid line demonstrates the boundary of the flux-rope region. The over-plotted black solid lines are the fitting curves of the VMGH model. Right: the top panel is the histogram of ω, the middle panel represents the correlation between B_ϕ/B_z and x, and the bottom panel presents the correlation between the modelled and measured B_ϕ/B_z.

cloud interval. The distribution of ω_i is shown in the top-right panel of Fig. 1. The scattering of ω_i is due to random fluctuations and small-scale features in the measured magnetic field. Similarly, the middle-right panel in Fig. 1 demonstrates the correlation between B_ϕ/B_z and x. The minor data points near the two ends of ω_i are biased, so to reduce this bias we select the data points that fall within 90 per cent significance (for detailed information, see Wang et al. 2015, 2016).

The derived ω distribution in the top-right panel of Fig. 1 indicates the best-fitting condition. It demonstrates a peak along with the half-maximum value on left and right (two vertical blue dashed lines). The model estimates $\omega = -3.52 \pm 1.71$. The middle-right and bottom-right panels of Fig. 1 show the variation of the B_ϕ/B_z versus x (i.e. normalized distance from the axis of the flux rope) and modelled B_ϕ/B_z versus measured B_ϕ/B_z, respectively. In the middle-right panel, the horizontal solid line corresponds to $\omega = -3.52$ with the limits of uncertainty shown by dashed lines. The blue data points are within the uncertainty limits. In the demonstrated case, about 63.5 per cent of the selected data points are within the uncertainty limits, the coefficient of correlation (cc) between the modelled and measured B_ϕ/B_z data points is 0.44, and the confidence level of the correlation under test is about 100 per cent. All these output parameters give the information about the goodness of fit for the model (i.e. how close the modelled output and magnetic field lines are to each other). The goodness of fit (χ_n) is also calculated for each flux rope listed in Table 1. It gives us the information about the overall relative uncertainty between the modelled and the observed values. A detailed explanation of χ_n is given in Wang et al. (2015, 2016). Table 1 presents the list of VMGH model output parameters of 26 ICME flux ropes observed by the *Helios* 1 and 2 spacecraft.

3 VARIATION OF DERIVED PARAMETERS AND DISCUSSION

3.1 Poloidal velocity (V_{pol})

The existence of the strong field-aligned streams of suprathermal electrons in ICME flux ropes (Larson et al. 1997) and the frequently observed plasma flows in prominences and coronal loops in the solar corona give a hint about the presence of poloidal motion in flux ropes. The study of poloidal motion will shed some light on the kinematic and thermodynamic evolution of CMEs (Wang, Zhang & Shen 2009; Zhao et al. 2017a; Mishra & Wang 2018). Wang et al. (2015) carried out a specific study to understand the poloidal motion of the flux ropes using a velocity-modified cylindrical force-free flux rope model. They explicitly investigated events that show almost

Table 1. Physical parameters of the 26 studied magnetic clouds/flux ropes derived by the VMGH model. The second column gives the spacecraft used for the magnetic cloud study, where H1 and H2 denote *Helios* 1 and 2, respectively. Columns 3 and 4 are the date and time (in h) of the magnetic cloud crossing, and column 5 is the magnetic cloud transit interval observed by the spacecraft. Column 6 denotes the position of the spacecraft in the heliosphere (in au). Columns 7–22 are the VMGH modelled output parameters. B_0 and R are the axial magnetic field strength and radius of the cross-section of the flux rope in units of nT and au. The elevation and azimuth angle of the flux-rope axis are represented by θ and ϕ. The flux-rope twist is shown by τ in units of turns au^{-1}. d is the closest approach of the observational path to the flux-rope axis in units of R. V_x, V_y and V_z are the propagation speed along the $\hat{x}$, $\hat{y}$ and $\hat{z}$ directions, while V_e and V_p are the expansion and poloidal speeds in the direction of $\hat{r}$ and $\hat{\varphi}$ of the studied flux ropes in units of km s^{-1}. The axial (F_z) and poloidal (F_ϕ) magnetic flux are in units of Mx, while the magnetic helicity (H_m) of the flux rope is in units of Mx^2. E_{m0} is the total magnetic energy of the flux rope (in erg). The normalized root-mean-square (rms) of the difference between the modelled and observed results is shown by χ_n.

Sr	SC	Magnetic cloud			Dist.	Modelled parameters														
No.		Date	Start	Δt	(au)	B_0	R	θ (°)	ϕ (°)	τ	d	V_x	V_y	V_z	V_e	V_p	F_z	F_ϕ	H_m	E_{m0}	χ_n
1	H1	1975/03/04	16.20	11.82	0.38	120.70	0.06	−0.39	54.94	$-3.52^{+3.9}_{-4.1}$	0.53	−464.49	6.66	−14.16	33.52	6.19	$1.78^{+1.48}_{-1.57}$	1.50E+22	−2.66E+43	6.06E+25	0.43
2	H2	1978/04/16	18.60	06.60	0.42	101.93	0.08	−28.90	98.24	$-1.34^{+0.2}_{-0.2}$	0.89	−507.42	−62.30	−69.94	77.03	85.68	$4.08^{+2.59}_{-2.34}$	1.31E+22	−5.35E+43	1.19E+26	0.16
3	H1	1979/05/28	23.40	12.24	0.43	79.88	0.06	−14.61	131.85	$-0.81^{+0.2}_{-0.2}$	−0.45	−518.24	10.63	−5.95	0.04	−22.33	$2.19^{+0.05}_{-0.05}$	4.58E+21	−1.00E+43	5.70E+25	0.48
4	H1	1981/05/26	02.28	29.16	0.47	65.06	0.14	56.82	134.61	$-0.46^{+0.1}_{-0.1}$	0.25	−476.70	26.81	−7.86	69.47	9.69	$7.70^{+0.19}_{-0.21}$	7.94E+21	−6.12E+43	1.23E+26	0.39
5	H2	1976/03/30	08.64	15.36	0.47	76.93	0.07	−45.37	215.53	$4.20^{+2.3}_{-2.3}$	0.50	−456.37	4.09	−2.12	21.29	7.46	$1.16^{+0.61}_{-0.61}$	1.20E+22	1.39E+43	2.65E+25	0.43
6	H2	1977/04/05	18.30	03.54	0.47	42.83	0.02	30.21	48.32	$-0.29^{+1.4}_{-1.4}$	−0.09	−457.78	−27.30	0.50	−2.80	−12.96	$0.07^{+0.00}_{-0.00}$	5.49E+19	−4.03E+39	1.04E+24	0.40
7	H1	1980/06/20	02.40	14.40	0.53	72.78	0.05	23.77	225.39	$-1.56^{+0.8}_{-0.7}$	−0.52	−409.07	−24.19	−37.08	54.89	4.47	$1.33^{+0.15}_{-0.15}$	4.62E+21	−6.13E+42	2.39E+25	0.38
8	H1	1978/11/29	05.76	05.04	0.55	52.32	0.05	14.61	284.69	$0.67^{+1.0}_{-1.0}$	−0.10	−799.54	51.03	−69.30	20.11	−17.61	$0.73^{+0.04}_{-0.04}$	1.24E+21	9.07E+41	1.19E+25	0.43
9	H1	1977/03/17	01.80	04.20	0.6	14.38	0.04	23.29	314.61	$0.07^{+0.2}_{-0.2}$	−0.93	−374.12	−3.57	−6.79	10.72	−2.40	$0.16^{+0.00}_{-0.00}$	3.00E+19	4.80E+39	7.30E+23	0.16
10	H2	1978/04/02	03.72	03.06	0.61	63.35	0.03	17.03	210.39	$4.32^{+0.7}_{-0.7}$	0.98	−378.73	−52.61	81.53	36.99	−100.00	$0.25^{+0.01}_{-0.01}$	2.64E+21	6.60E+41	4.68E+24	0.15
11	H1	1981/05/11	15.00	13.80	0.66	95.75	0.10	22.23	60.39	$-1.21^{+0.3}_{-0.3}$	−0.37	−792.66	−49.58	54.84	140.20	27.23	$5.43^{+0.57}_{-0.55}$	1.42E+22	−7.72E+43	1.20E+26	0.49
12	H2	1979/04/03	03.84	13.92	0.67	67.80	0.02	0.39	203.91	$3.35^{+1.1}_{-1.1}$	0.52	−422.21	−44.57	−15.22	7.64	−30.52	$0.25^{+0.02}_{-0.02}$	2.09E+21	5.33E+41	5.12E+24	0.22
13	H1	1977/12/01	14.16	08.40	0.75	37.37	0.04	−0.58	140.36	$-2.56^{+0.9}_{-1.1}$	−0.63	−428.26	−13.93	−4.53	17.37	−36.05	$0.28^{+0.03}_{-0.03}$	1.78E+21	−5.05E+41	3.15E+24	0.38
14	H1	1981/04/27	08.88	03.00	0.79	34.34	0.02	−60.39	314.61	$-0.91^{+0.4}_{-0.4}$	0.12	−555.86	−20.81	−10.49	4.45	16.81	$0.09^{+0.00}_{-0.00}$	2.01E+20	−1.75E+40	9.57E+23	0.30
15	H1	1981/04/27	17.64	09.96	0.79	32.23	0.05	−31.89	119.61	$-0.93^{+0.2}_{-0.2}$	−0.32	−438.36	12.53	20.78	34.33	2.96	$0.47^{+0.005}_{-0.005}$	1.04E+21	−4.94E+41	4.25E+24	0.22
16	H1	1981/01/27	18.00	07.56	0.85	19.19	0.05	35.67	29.61	$0.13^{+0.2}_{-0.2}$	−0.47	−632.36	19.68	33.24	20.67	−56.70	$0.29^{+0.00}_{-0.00}$	9.70E+19	2.89E+40	1.73E+24	0.29
17	H2	1978/12/24	14.40	11.16	0.85	20.68	0.06	−41.13	44.61	$-1.52^{+0.3}_{-0.2}$	0.69	−383.69	−3.19	40.17	−8.86	−17.87	$0.43^{+0.02}_{-0.02}$	1.72E+21	−7.41E+41	3.04E+24	0.29
18	H1	1975/11/17	11.04	06.84	0.87	12.99	0.06	10.61	74.28	$-0.22^{+0.0}_{-0.0}$	−0.87	−356.29	8.86	2.17	8.20	−28.14	$0.30^{+0.00}_{-0.00}$	1.66E+20	−4.97E+40	1.24E+24	0.20
19	H1	1981/04/14	04.20	20.76	0.89	12.20	0.17	23.13	314.61	$0.11^{+0.0}_{-0.0}$	0.79	−607.99	51.45	65.46	93.47	6.29	$2.32^{+0.00}_{-0.00}$	5.61E+20	1.30E+42	7.29E+24	0.26
20	H1	1975/01/07	02.76	08.16	0.92	43.69	0.09	−36.42	45.39	$-2.63^{+1.3}_{-1.3}$	0.80	−668.72	−12.61	−4.38	42.48	−54.24	$1.22^{+0.47}_{-0.47}$	7.87E+21	−9.60E+42	1.59E+25	0.47
21	H1	1980/08/04	22.80	02.40	0.93	9.92	0.01	−6.71	119.61	$-3.40^{+0.7}_{-0.7}$	−0.64	−347.80	−15.26	−4.96	11.27	35.35	$0.009^{+0.00}_{-0.00}$	7.36E+19	−6.38E+38	2.65E+22	0.15
22	H1	1979/03/03	09.96	06.72	0.94	37.83	0.11	45.39	96.96	$-0.63^{+0.1}_{-0.2}$	−0.90	−643.05	−38.87	0.52	75.19	7.10	$3.00^{+0.11}_{-0.12}$	4.60E+21	−1.38E+43	3.35E+25	0.24
23	H1	1977/01/29	12.30	08.10	0.95	29.43	0.10	73.62	68.67	$0.12^{+0.0}_{-0.0}$	−0.90	−480.29	−29.69	−10.40	60.66	−3.23	$1.98^{+0.003}_{-0.003}$	5.96E+20	1.18E+42	1.70E+25	0.15
24	H2	1978/01/06	01.44	05.46	0.95	12.15	0.03	0.39	240.39	$1.26^{+0.2}_{-0.2}$	−0.35	−583.25	−8.19	−2.71	15.67	−1.00	$0.096^{+0.00}_{-0.00}$	3.03E+20	2.93E+40	3.62E+23	0.52
25	H2	1978/02/16	02.64	30.36	0.95	15.76	0.08	−58.40	227.76	$-0.17^{+0.0}_{-0.0}$	−0.92	−453.00	−21.34	2.94	18.43	12.51	$0.75^{+0.001}_{-0.001}$	3.20E+20	−2.42E+41	3.75E+24	0.15
26	H1	1979/02/27	10.80	02.16	0.96	27.28	0.06	−30.97	231.51	$0.50^{+0.1}_{-0.1}$	0.98	−601.65	10.33	−98.71	−11.79	−42.91	$0.66^{+0.006}_{-0.006}$	8.60E+20	5.70E+41	5.96E+24	0.11

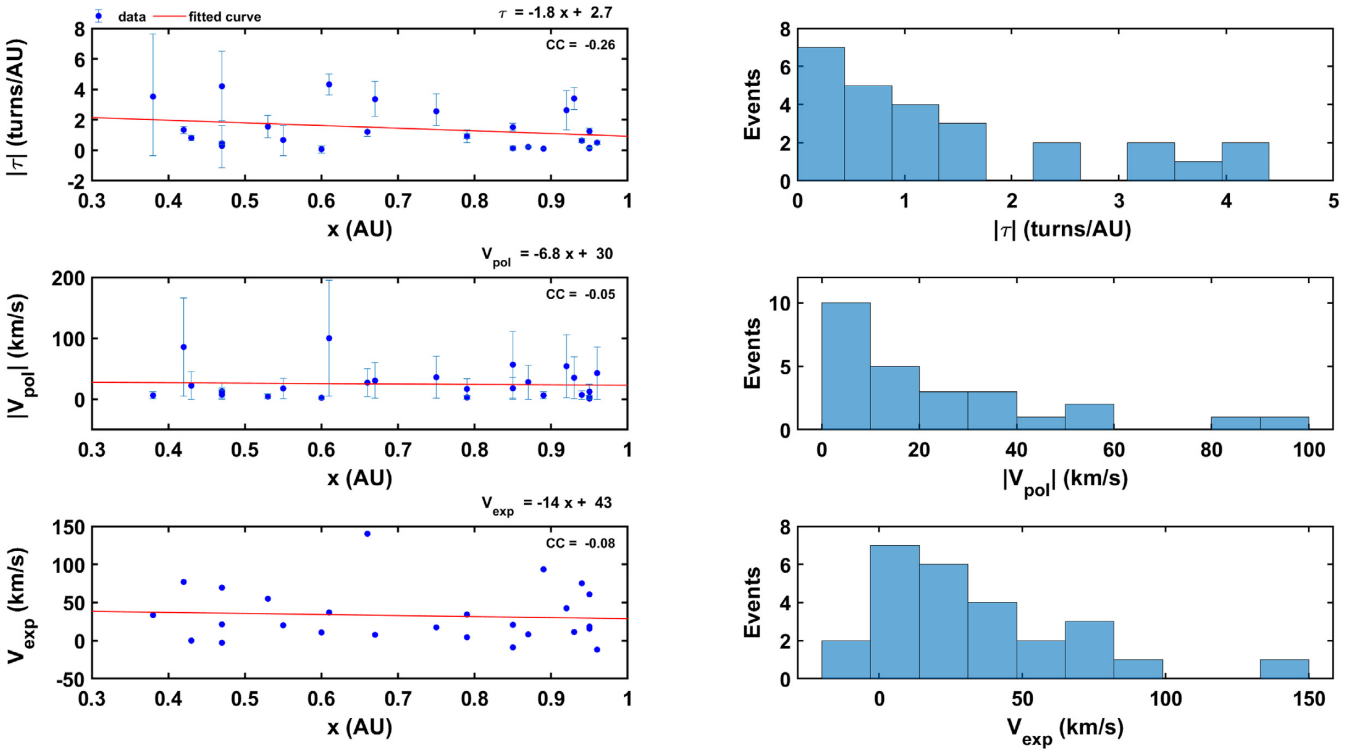

Figure 2. Left: variations of different physical parameters at different heliocentric distances: twist, τ (top panel), poloidal velocity, $V_{\rm pol}$ (middle panel), expansion velocity, $V_{\rm exp}$ (bottom panel), of the 26 studied flux-rope events as listed in Table 1. Right: the corresponding distributions of the events.

zero expansion speed (these events occurred on 2009 October 12 and 2003 March 20), and they noted that the poloidal speed of the ICME flux rope is –31 and 58 km s^{-1}, respectively. This clearly proves the existence of poloidal motion in the flux rope.

The middle-left panel of Fig. 2 indicates the variation of poloidal velocity in the flux rope with respect to heliocentric distance where they are observed by *Helios*. A very poor correlation coefficient close to zero (−0.05) is found. This unambiguously shows that the poloidal speed is completely independent with respect to the heliocentric observational location. In our analysis, the histogram (distribution plot) of the amplitude of poloidal speed shows that about 38.46 per cent of the events have poloidal speed between 0 and 10 km s^{-1}, while about 19.23 and 11.54 per cent of the events have a speed between 10–20 and 30–40 km s^{-1}. The median value of the absolute poloidal speed in the flux rope for our chosen sample is about 17.21 km s^{-1}. Wang et al. (2015) estimated that the median of poloidal speed is about 10 km s^{-1} at 1 au. Our estimated results are very consistent with their results even though Wang et al. (2015) used a velocity-modified Lundquist solution, while we have used the VMGH solution. The non-zero poloidal motion suggests that flux ropes carry non-zero angular momentum. This angular momentum can be generated internally all the time of the CME from its early phase in the corona to the propagation phase in interplanetary space, and/or generated locally through the interaction with ambient solar wind, and/or generated initially at the eruption of the CME in the corona and carried all the way to the heliosphere (Wang et al. 2015). As we have observed no significant correlation between poloidal motion and heliocentric distance, the poloidal motion is probably caused locally, as suggested in a case study by Zhao et al. (2017a, 2017b). Moreover, this study clearly indicates that, in addition to the expansion speed, the poloidal speed has significant importance for studies of flux-rope evolution. If the poloidal motion is generated during the eruption of a CME-associated flux rope at the Sun, it is possible that the poloidal speed decreased quickly to reach an asymptotic value as the CME propagated in the corona. In a recent study by Mishra & Wang (2018), it is shown that centrifugal force due to poloidal motion decreases faster than Lorentz and thermal pressure force as the CME moves a couple of solar radii from the Sun.

3.2 Expansion velocity ($V_{\rm exp}$)

The *in situ* observations of the solar wind velocity profile, during the ICME flux-rope cross-over, shows a linear and gradual decrease in their respective speed. This is attributed to the self-similar expansion of the flux rope (Farrugia et al. 1993; Shimazu & Vandas 2002; Démoulin et al. 2008; Démoulin & Dasso 2009a). In the present study, using the VMGH model, we estimated the expansion speed of the selected ICMEs, which were observed at different locations in the heliosphere by the *Helios* 1 and 2 spacecraft. The variation with respect to heliocentric distance is shown in the bottom-left panel of Fig. 2. A very poor correlation coefficient (i.e. −0.08) is found between them. This suggests that the expansion speed of the flux rope converged to an almost constant speed before crossing out a few tens of solar radii from the Sun. The linear regression relation suggests a slow gradual decrease in expansion speed with a slope of about −14 km s^{-1} au^{-1} and an upper cut-off of about 43 km s^{-1}. The distribution plot of the expansion velocity shows a peak in velocity range −3 to 14 km s^{-1}, which is about 26.92 per cent of events. In fact, the distribution shows a contraction of flux rope (negative expansion velocity) for 11.54 per cent of the ICME cross-over events with the highest contraction of $V_{\rm e} \simeq -11.79$ km s^{-1}. Similar to our study, Wang et al. (2015) suggested that a significant fraction of events (i.e. 26 per cent at 1 au) indicates contraction in the

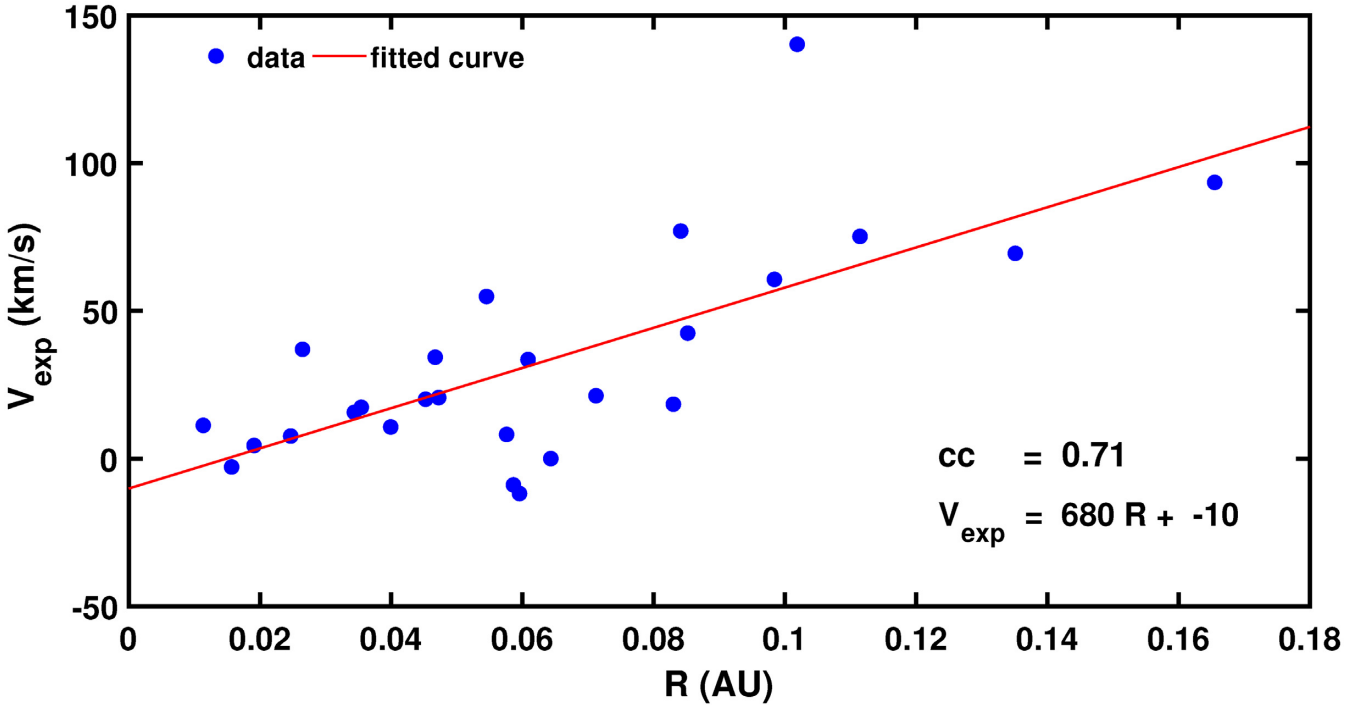

Figure 3. Scattered plot of the expansion velocity (V_{exp}) of 26 magnetic clouds/flux ropes with respect to the radius (R) of the flux rope.

flux rope with a median contraction speed of about 12 km s^{-1}. The significant contraction may occur when the solar wind speed at the leading edge of the flux rope is smaller than that of the rear edge of flux rope and/or a faster solar wind stream pushes the rear edge from the back. In fact, sometimes contraction also occurs when the flux rope is overtaken by the faster solar wind stream (Wang et al. 2015).

Besides this, we clearly observe a decreasing trend in the number of events with respect to an increase in expansion velocity. The observed median expansion velocity of flux ropes during this study is about 21.29 km s^{-1}, whereas Wang et al. (2015) found the median speed is about 21 km s^{-1}. Earlier studies (Lepping et al. 2003; Démoulin & Dasso 2009a; Wang et al. 2015) have suggested that the rapid decrease of the total solar wind pressure with heliocentric distance is the main driver of the flux-rope expansion at 1 au. Gulisano et al. (2010, 2012) also corroborated a similar result in the inner and outer heliosphere. Thus, our present results using the VMGH model for sub-au regions are consistent with previous studies of the expansion and contraction of the flux rope in interplanetary space.

Fig. 3 demonstrates the dependence of flux-rope size on the expansion speed. The Pearson correlation coefficient (cc) between these two parameters is estimated to be 0.71, which is significantly high. The regression analysis clearly suggests a linear relation between the size of the flux rope and the expansion velocity. It implies that the expansion speed increases as size of the flux rope increases, and vice versa.

Moreover, Gopalswamy et al. (2014) found that the CMEs in cycle 24 experienced 'anomalous expansion' compared with those in cycle 23. They suggested that V_{exp} is affected by a change in the ambient medium (i.e. decreased total pressure of the heliosphere in cycle 24). This seems to contradict our results that the internal properties of the flux rope are dominant for V_{exp}. In addition, Gopalswamy et al. (2015) found that V_{exp} of magnetic clouds in cycle 24 is smaller than that in cycle 23, consistent with the diminished difference between the magnetic cloud and the ambient total pressure in cycle 24. They suggested that the increased CME expansion in cycle 24 occurred near the Sun and resulted in a larger pressure–balance distance ($\sim$12 R in cycle 24 versus $\sim$5 R in cycle 23). Moreover, in our analysis the measurements are made in interplanetary space, well above the solar corona where the measurements of Gopalswamy et al. (2014) were made, which showed the anomalous expansion of CMEs in cycle 24.

3.3 Poloidal magnetic flux F_ϕ

The variation of the poloidal magnetic flux of the studied flux ropes observed at different heliospheric distances is shown in the top-left panel of Fig. 4. It demonstrates a decreasing trend; that is, flux measured at larger distances from the Sun is found to be smaller with a power-law fit $F_\phi = 0.09x^{-2.8}$. The continuous interaction with ambient solar wind and the expansion of the flux rope can be attributed to the observed decreasing trend of the poloidal flux.

Recently, Wang et al. (2018) reported a rare ICME event, which was observed sequentially by four spacecraft near Mercury, Venus, Earth and Mars, respectively. They found that the axial magnetic flux and helicity of the ICME flux rope decreased during its outward propagation but the twist increased. The observed decreasing trend of poloidal flux with respect to heliospheric distance is consistent with the reported study and may be caused by the 'pancaking' effect and 'erosion' effect, as suggested by Wang et al. (2018).

The correlation coefficient between the poloidal flux and heliospheric distance is about -0.57. The top-right panel of Fig. 4 shows the distribution. It peaks with 13 events (50.0 per cent) for $\simeq 1.5 \times 10^{22}$ Mx. It is also important to note that the distribution shows only a few events with high poloidal flux. This implies that

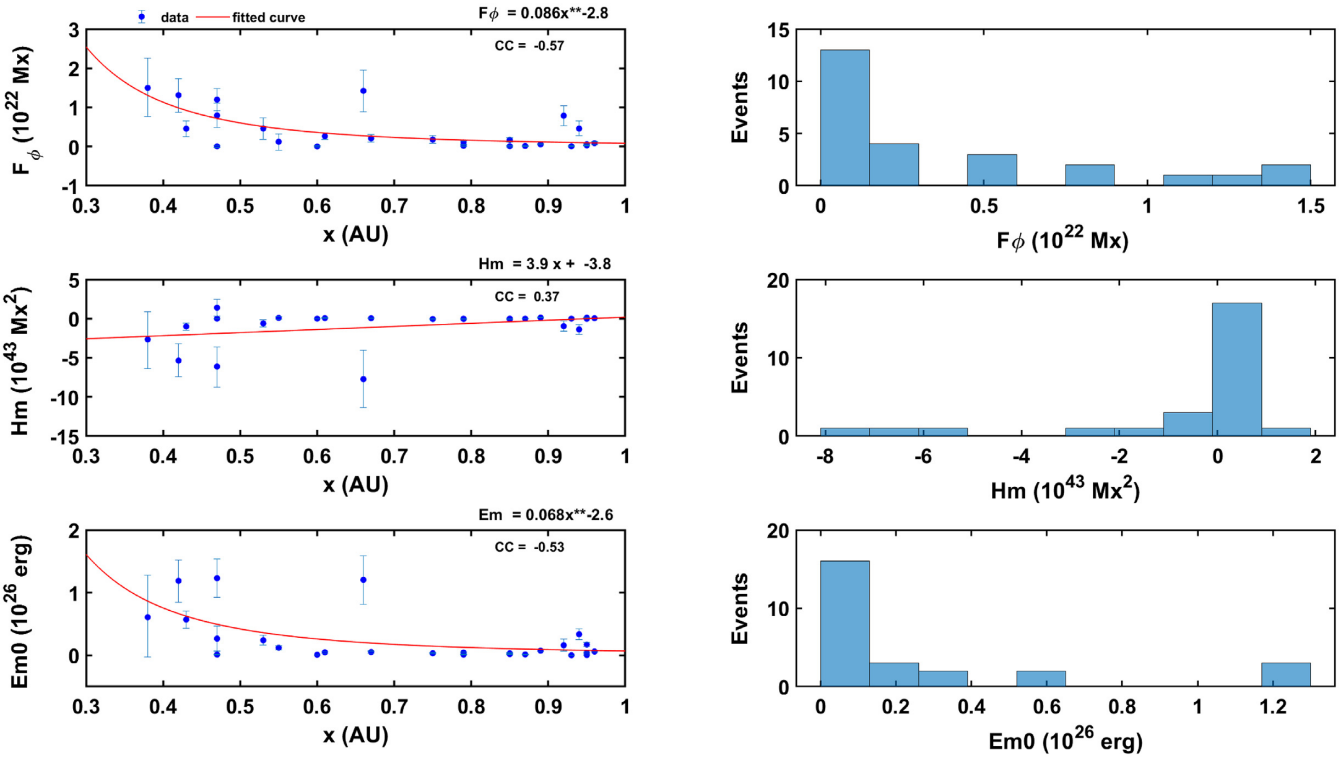

Figure 4. The left panel shows, from top to bottom, the spatial variation of the physical parameters: the poloidal magnetic flux F_ϕ, total magnetic helicity H_m and total magnetic energy E_m of the 26 studied magnetic cloud/flux rope events, as listed in Table 1. The right panel shows corresponding histogram plots of the above physical parameters.

most of the flux ropes in our sample are observed at relatively large distances and have less poloidal flux, whereas few flux ropes with high poloidal flux are observed. The median value of the poloidal flux is about 1.48×10^{21} Mx, which is in good agreement with the previous study (3.6×10^{21} Mx) done by Wang et al. (2015).

3.4 Magnetic helicity H_m

In the last couple of decades, many researchers have studied interplanetary flux ropes and their magnetic helicity (Dasso et al. 2003, 2005a; Nindos, Zhang & Zhang 2003; Gulisano et al. 2005; Luoni et al. 2005). In fact, interplanetary flux ropes are linked to solar phenomena by the conservation of magnetic helicity (Luoni et al. 2005; Mandrini et al. 2005). In the present study, the correlation coefficient of the magnetic helicity with that of heliospheric distance is about 0.37 whereas the estimated slope of the regression analysis is about 3.9 Mx^2 au^{-1} (see the middle-left panel of Fig. 4). However, it is important to note that the magnitude of helicity for flux ropes observed at lower heliospheric distances is high compared with measurements at 1 au. This is consistent with the study of Wang et al. (2015). It clearly indicates that the magnetic helicity of flux ropes is independent of heliocentric distance. Our analysis shows about 38.46 per cent of the events have positive polarity while the remaining 61.54 per cent have negative polarity. The median value of absolute magnetic helicity for the studied events is about 0.7×10^{42} Mx^2. DeVore (2000) studied the helicity of 18 ICME flux ropes using the classical Lundquist (1950) model and the estimated value was $\sim 2 \times 10^{42}$ Mx^2. Similarly, Dasso et al. (2005b) found the average helicity of eight studied flux ropes to be 2.57×10^{42} Mx^2. Further, Wang et al. (2015) estimated the average helicity to be about 2.05×10^{42} Mx^2 by investigating 72 magnetic clouds. The results of the present work are very consistent with the reported studies, even though all previous studies were performed at 1 au.

3.5 τ (twist/au)

Hu et al. (2015) suggested that flux ropes are likely to be uniformly twisted except for the region very close to the axis. Therefore, it is believed that the VMGH model based on the uniform twist of flux ropes is one of the best solutions to determine their characteristics (Wang et al. 2016). It is emphasized that different flux-rope structures in our chosen sample are observed by the *Helios* spacecraft at different locations between 0.3 and 0.9 au. Thus, the modelled flux-rope parameters over a range of radial distances in the heliosphere can give an insight into the evolution of the parameters in a statistical sense. The top panel in Fig. 2(a) shows the variation in the number of turns per unit length in the magnetic field lines along the axis of the flux rope (τ) with heliospheric distances where the distinctly observed 26 ICME flux ropes are sampled by the *Helios* spacecraft, as listed in Table 1. The correlation coefficient between estimated τ and heliospheric distance (observational location of the flux rope) is -0.26. This indicates that the twist of the individual flux ropes is almost independent of the heliocentric distance. However, the estimated twist shows large scatter around the linear regression line. The slope of the linear relation is -1.80 turns au^{-1} and the upper limit of the twist is 2.7 turns au^{-1}. The twist distribution of the 26 flux ropes is shown in the top-right panel of Fig. 2. The output of the distribution is summarized in Table 2. About 26.92 per cent of events lie between 0 and 0.44 turns au^{-1}, while 19.23 and 15.38 per cent of the events have twist between 0.44 and 0.88 turns au^{-1} and between 0.88 and 1.32 turns au^{-1}, respectively. We observe that the number of events decreases with the increase in the twist. The trends

Table 2. Detailed description of the bin size of different flux-rope parameters and their distribution.

Histogram distribution of the 26 ICME flux-rope events			
Parameters	Bin size	Events out of 26	Per cent
τ turns au^{-1}	0.00–0.44	7	**26.92**
	0.44–0.88	5	**19.23**
	0.88–1.32	4	**15.38**
	1.32–1.76	3	**11.54**
	1.76–2.20	0	00.00
	2.20–2.64	2	07.69
	2.64–3.08	0	00.00
	3.08–3.52	2	07.69
	3.52–3.96	1	03.85
	3.96–4.40	2	07.69
V_p (km s^{-1})	0–10	10	**38.46**
	10–20	5	**19.23**
	20–30	3	**11.54**
	30–40	3	**11.54**
	40–50	1	03.85
	50–60	2	07.69
	60–70	0	00.00
	70–80	0	00.00
	80–90	1	03.85
	90–100	1	03.85
V_e (km s^{-1})	(−20)–(−3)	2	07.69
	(−3)–14	7	**26.92**
	14–31	6	**23.08**
	31–48	4	**15.38**
	48–65	2	07.69
	65–82	3	**11.54**
	82–99	1	03.85
	99–116	0	00.00
	116–133	0	00.00
	133–150	1	03.85
F_ϕ (Mx)	0.00–1.5	13	**50.00**
	1.5–3.0	4	**15.38**
	3.0–4.5	0	00.00
	4.5–6.0	3	**11.54**
	6.0–7.5	0	00.00
	7.5–9.0	2	07.69
	9.0–10.5	0	00.00
	10.5–12.0	1	03.85
	12.0–13.5	1	03.85
	13.5–15.0	2	07.69
H_m (Mx^2)	(−8.10)–(−7.10)	1	03.85
	(−7.10)–(−6.10)	1	03.85
	(−6.10)–(−5.10)	1	03.85
	(−5.10)–(−4.10)	0	00.00
	(−4.10)–(−3.10)	0	00.00
	(−3.10)–(−2.10)	1	03.85
	(−2.10)–(−1.10)	1	03.85
	(−1.10)–(−0.10)	3	**11.54**
	(−0.10)–(0.90)	17	**65.38**
	(0.90)–(1.90)	1	03.85
E_{m0} (erg)	0.00–0.13	16	**61.53**
	0.13–0.26	3	**11.54**
	0.26–0.39	2	07.69
	0.39–0.52	0	00.00
	0.52–0.65	2	07.69
	0.65–0.78	0	00.00
	0.78–0.91	0	00.00
	0.91–1.04	0	00.00
	1.04–1.17	0	00.00
	1.17–1.30	3	**11.54**

of the histogram plots indicate that the events fitted by the VMGH model are consistent with previous studies (Wang et al. 2016).

In fact, various techniques have been used to estimate the twist of the magnetic flux rope in the past. Farrugia et al. (1999) were the first to utilize the GH model to fit samples of the observed magnetic flux ropes and found that the twist is about ∼8 turns au^{-1}, which is significantly larger than the values of the twist derived for the observed flux rope in our sample. Dasso et al. (2006) evaluated the twist of flux ropes by using the GH model and reported a twist of about ∼2.4 turns au^{-1}. Möstl et al. (2009) used GS reconstruction technique for multispacecraft data and found that the average twist of the flux rope is about ∼1.5 to ∼1.7 turns au^{-1}. In addition, Kahler et al. (2011) studied the twist of the flux rope using an energetic electron probe and suggested a change in the twist from the axis to the edge of the flux rope. This is further corroborated by Hu et al. (2014, 2015), who estimated the twist of the flux rope by GS reconstructions and further concluded that the average twist varies between ∼1.7 and ∼7.7 turns au^{-1}.

We have also studied the relations between the τ and R (flux-rope radius) values of the flux rope (see Fig. 5) for all the studied events. The two dashed lines in Fig. 5 demonstrate the upper and lower boundaries and the spine of these data points corresponds to ω values of 2.0 and 0.5, respectively. We noticed that flux ropes that have a thickness (radius) greater than 0.1 au possess less twist (*i.e.* below or close to the HP critical twist), suggesting that they are not susceptible to kink instability. Interestingly, almost half of the flux-rope events with thickness below 0.1 au have a higher twist than the HP critical twist. This clearly implies that thinner flux ropes have almost 50 per cent probability to be deformed under kink instability. Moreover, the higher twist may put a limit on the expansion and size of the flux rope. In our study, the twists of the events roughly follow $0.5/2\pi R$, which is equivalent to $\Phi_T = 0.5l/R$, and they are well bounded by the line of $\omega = 2.0$ (i.e. $\Phi_T = 2l/R$), as found by Wang et al. (2016).

3.6 Magnetic energy E_{m0}

It is important to estimate the initial magnetic energy budget of the flux ropes at different heliospheric distances. Vourlidas et al. (2010) suggested that the initial magnetic energy of a flux rope is about 2.84×10^{31} erg, which is ten times greater than their kinetic energy (i.e. $10^{29}-10^{30}$ erg). The bottom-left panel of Fig. 4 shows that the estimated initial magnetic energy is smaller for a flux rope observed at a larger distance from the Sun. The variations of magnetic energy with heliospheric distance display power-law behaviour with the spectral index of −2.6. Moreover, the correlation coefficient between them is −0.53. Previous studies suggest that the expansion of the ICME decreases the associated magnetic energy of the CME (Kumar & Rust 1996; Wang et al. 2009; Nakwacki et al. 2011). It is also understood that the magnetic energy converts into either thermal energy or kinetic energy through some physical mechanisms during the propagation of flux ropes. In fact, magnetic

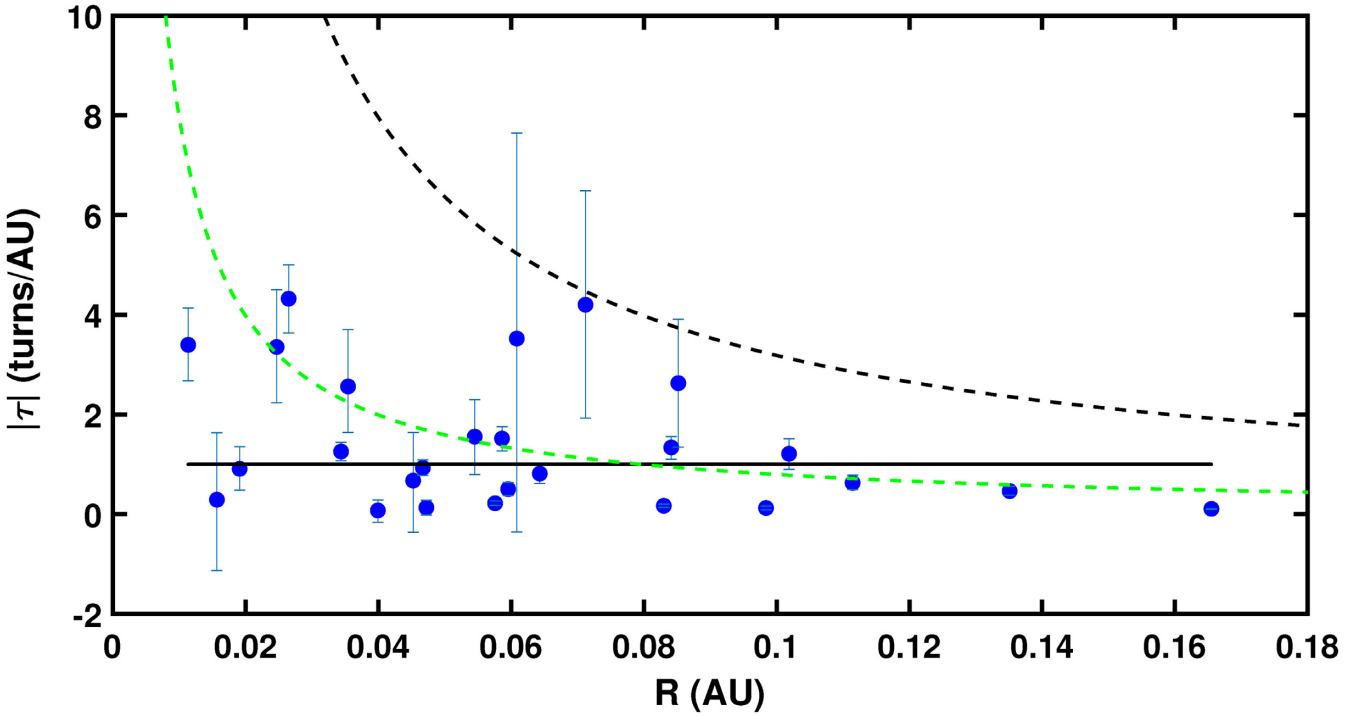

Figure 5. Scattered plot of the twist (τ) with respect to the radius (R) of the flux rope. The dashed line gives $\tau = \omega/(2\pi R)$ for different values of ω = 2.0 (black dashed line) and 0.5 (green dashed line). The solid line denotes the HP critical twist (i.e. the twist at which the flux rope becomes kink-unstable), which is taken as 1.25 (Hood & Priest 1981).

energy plays a key role in the expansion of the flux ropes. Their distribution plot indicates that 62 per cent of events have total magnetic energy below 0.13×10^{26} erg, while only about 11.54 per cent of the events have energy from 0.13×10^{26} to 0.26×10^{26} erg and from 1.17×10^{26} to 1.30×10^{26} erg, respectively. The median initial magnetic energy of the studied events is about 0.5×10^{25} erg. It is also proposed that the conversion of magnetic energy into rotational kinetic energy could be responsible for the existence of poloidal motion (Wang et al. 2015). Besides, the 'pancaking' effect and 'erosion' effect are strongly contributing to the observed trend of total energy (Wang et al. 2018).

4 CONCLUSION

The conclusions drawn from our investigation of flux-rope characteristics by fitting the VMGH model to the measurements of the *Helios* 1 and 2 spacecraft are the following.

(i) The distribution of τ shows that about ∼73 per cent of the flux ropes have twist ≤1.76 turns au^{-1}, whereas the maximum twist observed is ∼4.30 turns au^{-1}. The strongly twisted magnetic field lines probably limit the expansion and size of a flux rope (Wang et al. 2016).The near-zero correlation coefficient implies that the twist is independent of heliocentric distance.

(ii) The present study explicitly suggests that ∼81 per cent of flux ropes have poloidal speed ≤ 40 km s^{-1} whereas ∼38 per cent have a speed ≤ 10 km s^{-1}. The poor correlation coefficient with heliocentric distance implies that the poloidal motion of flux ropes may be generated during their respective ejection process.

(iii) The other important result noted during the study was the power-law decreasing trend of the poloidal flux with heliocentric distance. The spectral index is about −2.8. About 50 per cent of the events have poloidal flux of 1.5×10^{22} Mx.

(iv) Our results suggest that the internal properties of the flux rope are dominant for V_{exp}. This is in contrast to Gopalswamy et al. (2014), who explain the 'anomalous expansion' of flux ropes during solar cycle 24 compared with those in cycle 23 by a decreased total pressure of the heliosphere.

(v) It is observed that the expansion and/or contraction of 26 flux ropes is independent of heliocentric distance. Interestingly, it is noted that about 11.54 per cent of the events shows contraction while remaining 88.46 per cent of the flux ropes shows expansion. This implies that when ICME flux rope evolves in interplanetary space it expands more than contracts.

(vi) About ∼61 per cent (16 out of 26 flux ropes) of the flux ropes indicate that the topology of the magnetic flux rope is left-hand polarized and 39 per cent of the flux ropes are right-hand polarized.

(vii) Most of the time (about ∼61 per cent of flux ropes), we observe that the initial magnetic energy of the flux ropes is below 0.13×10^{26} erg. Further, the initial magnetic energy follows a power-law decreasing trend with spectral index −2.8. This indicates that the magnetic energy decreases with the distance from the Sun.

ACKNOWLEDGEMENTS

We are thankful to the *Helios* spacecraft data providers for making interplanetary data available at https://cdaweb.gsfc.nasa.gov/pub/data/helios/. AR also thanks the Solar-TErrestrial Physics (STEP) group, the University of Science and Technology of China and the Scientific Committee on STEP (SCOSTEP) Visiting Scholar Programme. YW is supported by the National Natural Science Foundation of China (NSFC) grant Nos 41774178 and 41761134088. WM is supported by the Chinese Academy of Sciences (CAS) President's International Fellowship Initiative (PIFI) grant No. 2015PE015 and by the NSFC grant No. 41750110481.

REFERENCES

Al-Haddad N., Roussev I., Möstl C., Jacobs C., Lugaz N., Poedts S., Farrugia C., 2011, ApJ, 738, L18
Al-Haddad N. et al., 2013, Solar Phys., 284, 129
Berdichevsky D., Lepping R., Farrugia C., 2003, Phys. Rev. E, 67, 036405
Bothmer V., Schwenn R., 1994, in Fleck B., Noci G., Poletto G., eds, Mass Supply and Flows in the Solar Corona. Springer, Berlin, p. 215
Bothmer V., Schwenn R., 1998, Ann. Geophys., 16, 1
Burlaga L., 1988, J. Geophys. Res.: Space Phys., 93, 7217
Burlaga L. F., 1991, in Schwenn R., Marsch E., eds, Physics of the Inner Heliosphere II: Particles, Waves and Turbulence. Springer, Berlin, p. 1
Burlaga L., Sittler E., Mariani F., Schwenn R., 1981, J. Geophys. Res.: Space Phys., 86, 6673
Dasso S., Mandrini C., Démoulin P., Farrugia C., 2003, J. Geophys. Res.: Space Phys., 108, 1362
Dasso S., Gulisano A., Mandrini C., Démoulin P., 2005a, Adv. Space Res., 35, 2172
Dasso S., Mandrini C. H., Démoulin P., Luoni M. L., Gulisano A. M., 2005b, Adv. Space Res., 35, 711
Dasso S., Mandrini C. H., Démoulin P., Luoni M. L., 2006, A&A, 455, 349
Dasso S., Nakwacki M., Démoulin P., Mandrini C., 2007, Solar Phys., 244, 115
Démoulin P., Dasso S., 2009a, A&A, 498, 551
Démoulin P., Dasso S., 2009b, A&A, 507, 969
Démoulin P., Nakwacki M. S., Dasso S., Mandrini C. H., 2008, Solar Phys., 250, 347
Démoulin P., Dasso S., Janvier M., 2013, A&A, 550, A3
DeVore C. R., 2000, ApJ, 539, 944
Farrugia C., Burlaga L., Osherovich V., Richardson I., Freeman M., Lepping R., Lazarus A., 1993, J. Geophys. Res.: Space Phys., 98, 7621
Farrugia C., Osherovich V., Burlaga L., 1995, J. Geophys. Res.: Space Phys., 100, 12293
Farrugia C. et al., 1999, in AIP Conf. Proc. Vol. 471, Solar Wind Conference. Am. Inst. Phys., New York, p. 745
Farrugia C. et al., 2005, in Fleck B., Zurbuchen T. H., Lacoste H., eds, ESA SP-592, Solar Wind 11/SOHO 16, Connecting Sun and Heliosphere. ESA Publications, Noordwijk, p. 723
Goldstein H., 1983, NASA Conference Publication, 228, 731
Gopalswamy N., Akiyama S., Yashiro S., Xie H., Mäkelä P., Michalek G., 2014, Geophys. Res. Lett., 41, 2673
Gopalswamy N., Yashiro S., Xie H., Akiyama S., Mäkelä P., 2015, J. Geophys. Res.: Space Phys., 120, 9221
Gosling J. T., 1990, Physics of Magnetic Flux Ropes, 58, 343
Gulisano A., Dasso S., Mandrini C., Démoulin P., 2005, J. Atmos. Solar-Terrestrial Phys., 67, 1761
Gulisano A. M., Démoulin P., Dasso S., Ruiz M. E., Marsch E., 2010, A&A, 509, A39
Gulisano A. M., Démoulin P., Dasso S., Rodriguez L., 2012, A&A, 543, A107
Hidalgo M., 2003, J. Geophys. Res.: Space Phys., 108, 1320
Hidalgo M., Nieves-Chinchilla T., 2012, ApJ, 748, 109
Hood A., Priest E., 1981, Geophysical & Astrophysical Fluid Dynamics, 17, 297
Hu Q., Sonnerup B. U., 2002, J. Geophys. Res.: Space Phys., 107, 1142
Hu Q., Qiu J., Dasgupta B., Khare A., Webb G., 2014, ApJ, 793, 53
Hu Q., Qiu J., Krucker S., 2015, J. Geophys. Res.: Space Phys., 120, 5266
Isavnin A., Vourlidas A., Kilpua E., 2013, Solar Phys., 284, 203
Isavnin A., Vourlidas A., Kilpua E. K., 2014, Solar Phys., 289, 2141
Jian L., Russell C., Luhmann J., Skoug R., 2006, Solar Phys., 239, 393
Kahler S., Krucker S., Szabo A., 2011, J. Geophys. Res.: Space Phys., 116, 1104
Kilpua E. et al., 2009, Ann. Geophys.: Atmospheres, Hydrospheres and Space Sciences, 27, 4491
Kilpua E., Koskinen H. E., Pulkkinen T. I., 2017, Living Reviews in Solar Physics, 14, 5
Klein L., Burlaga L., 1982, J. Geophys. Res.: Space Phys., 87, 613
Kumar A., Rust D., 1996, J. Geophys. Res.: Space Phys., 101, 15667
Larson D. et al., 1997, Geophys. Res. Lett., 24, 1911
Leitner M., Farrugia C., Möstl C., Ogilvie K., Galvin A., Schwenn R., Biernat H., 2007, J. Geophys. Res.: Space Phys., 112, 6113
Lepping R., Jones J., Burlaga L., 1990, J. Geophys. Res., 95, 11957
Lepping R., Berdichevsky D., Szabo A., Arqueros C., Lazarus A., 2003, Solar Phys., 212, 425
Lugaz N., 2010, Solar Phys., 267, 411
Luoni M., Mandrini C., Dasso S., van Driel-Gesztelyi L., Démoulin P., 2005, J. Atmos. Solar–Terrestrial Phys., 67, 1734
Mandrini C. H., Pohjolainen S., Dasso S., Green L., Démoulin P., van Driel-Gesztelyi L., Copperwheat C., Foley C., 2005, A&A, 434, 725
Marubashi K., 1986, Adv. Space Res., 6, 335
Marubashi K., 1997, in Crooker N., Joselyn J. A., Feynman J., eds, Geophys. Monogr. Ser. Vol. 99, Coronal Mass Ejections. American Geophysical Union, Washington DC, p. 147
Marubashi K., Lepping R., 2007, Ann. Geophys., 25, 2453
Marubashi K., Cho K-S., Kim Y-H., Park Y-D., Park S-H., 2012, J. Geophys. Res.: Space Phys., 117, 1101
Mishra W., Wang Y., 2018, ApJ, 865, 50
Moldwin M., 2008, An Introduction to Space Weather. Cambridge Univ. Press, Cambridge
Moldwin M., Phillips J., Gosling J., Scime E., McComas D., Bame S., Balogh A., Forsyth R., 1995, J. Geophys. Res.: Space Phys., 100, 19903
Möstl C., Farrugia C., Biernat H., Leitner M., Kilpua E., Galvin A., Luhmann J., 2009, Solar Phys., 256, 427
Mulligan T., Russell C., 2001, J. Geophys. Res.: Space Phys., 106, 10581
Nakagawa T., Matsuoka A., 2010, J. Geophys. Res.: Space Phys., 115, A10113
Nakwacki M. S., Dasso S., Démoulin P., Mandrini C. H., Gulisano A. M., 2011, A&A, 535, A52
Nindos A., Zhang J., Zhang H., 2003, ApJ, 594, 1033
Owens M. J., Merkin V., Riley P., 2006, J. Geophys. Res.: Space Phys., 111, 3104
Owens M., Démoulin P., Savani N., Lavraud B., Ruffenach A., 2012, Solar Phys., 278, 435
Owens M., Lockwood M., Barnard L., 2017, Scientific Reports, 7, 4152
Priest E. R., 1990, Physics of Magnetic Flux Ropes, 58, 1
Raghav A., Shaikh Z., Bhaskar A., Datar G., Vichare G., 2017, Solar Phys., 292, 99
Raghav A. N., Kule A., Bhaskar A., Mishra W., Vichare G., Surve S., 2018, ApJ, 860, 26
Raghav A. N., Shaikh Z. I., 2020, MNRASL, 493, L16
Romashets E., Vandas M., 2003, Geophys. Res. Lett., 30, 2065
Romashets E., Vandas M., 2009, A&A, 499, 17
Schwenn R., 2006, Living Reviews in Solar Physics, 3, 2
Shaikh Z., Raghav A., Bhaskar A., 2017, ApJ, 844, 121
Shimazu H., Vandas M., 2002, Earth, Planets and Space, 54, 783
Vandas M., Romashets E., 2003, A&A, 398, 801
Vourlidas A., Howard R. A., Esfandiari E., Patsourakos S., Yashiro S., Michalek G., 2010, ApJ, 722, 1522
Wang Y., Ye P., Wang S., Zhou G., Wang J., 2002, J. Geophys. Res.: Space Phys., 107, 1340
Wang Y., Shen C., Wang S., Ye P., 2004, Solar Physics, 222, 329
Wang C., Du D., Richardson J., 2005, J. Geophys. Res.: Space Phys., 110, A10107
Wang Y., Xue X., Shen C., Ye P., Wang S., Zhang J., 2006, ApJ, 646, 625
Wang Y., Zhang J., Shen C., 2009, J. Geophys. Res.: Space Phys., 114, A10104
Wang Y., Wang B., Shen C., Shen F., Lugaz N., 2014, J. Geophys. Res.: Space Phys., 119, 5117
Wang Y., Zhou Z., Shen C., Liu R., Wang S., 2015, J. Geophys. Res.: Space Phys., 120, 1543

Wang Y., Zhuang B., Hu Q., Liu R., Shen C., Chi Y., 2016, J. Geophys. Res.: Space Phys., 121, 9316
Wang W., Liu R., Wang Y., Hu Q., Shen C., Jiang C., Zhu C., 2017, Nature Communications, 8, 1330
Wang Y. et al., 2018, J. Geophys. Res.: Space Phys., 123, 3238
Zhang G., Burlaga L., 1988, J. Geophys. Res.: Space Phys., 93, 2511
Zhao A., Wang Y., Chi Y., Liu J., Shen C., Liu R., 2017a, Solar Phys., 292, 58
Zhao A., Wang Y., Liu J., Zhou Z., Shen C., Liu R., Zhuang B., Zhang Q., 2017b, ApJ, 845, 109
Zhao A., Wang Y., Feng H., Xu M., Zhao Y., Zhao G., Hu Q., 2018, ApJ, 869, L13

This paper has been typeset from a TEX/LATEX file prepared by the author.